

Solution-Processable Ultrathin Size- and Shape-Controlled Colloidal Cu_{2-x}S Nanosheets

Ward van der Stam,[†] Quinten A. Akkerman,[†] Xiaoxing Ke,[‡] Marijn A. van Huis,[§] Sara Bals,[‡] and Celso de Mello Donega^{*,†}

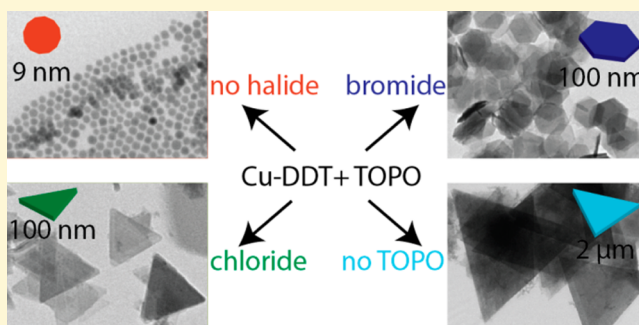
[†]Condensed Matter and Interfaces, Debye Institute for Nanomaterials Science, Utrecht University, Princetonplein 5, 3584 CC Utrecht, The Netherlands

[‡]Electron Microscopy for Materials Science (EMAT), University of Antwerp, Groenenborgerlaan 171, B-2020 Antwerp, Belgium

[§]Soft Condensed Matter, Debye Institute for Nanomaterials Science, Utrecht University, Princetonplein 5, 3584 CC Utrecht, The Netherlands

S Supporting Information

ABSTRACT: Ultrathin two-dimensional (2D) nanosheets (NSs) possess extraordinary properties that are attractive for both fundamental studies and technological devices. Solution-based “bottom-up” methods are emerging as promising routes to produce free-standing NSs, but the synthesis of colloidal NSs with well-defined size and shape has remained a major challenge. In this work, we report a novel method that yields 2 nm thick colloidal Cu_{2-x}S NSs with well-defined shape (triangular or hexagonal) and size (100 nm to 3 μm). The key feature of our approach is the use of a synergistic interaction between halides (Br or Cl) and copper-thiolate metal–organic frameworks to create a template that imposes 2D constraints on the Cu-catalyzed C–S thermolysis, resulting in nucleation and growth of colloidal 2D Cu_{2-x}S NSs. Moreover, the NS composition can be postsynthetically tailored by exploiting topotactic cation exchange reactions. This is illustrated by converting the Cu_{2-x}S NSs into ZnS and CdS NSs while preserving their size and shape. The method presented here thus holds great promise as a route to solution-processable compositionally diverse ultrathin colloidal NSs with well-defined shape and size.



INTRODUCTION

Ultrathin two-dimensional (2D) nanomaterials (nanosheets, NSs) are attracting increasing research efforts due to their extraordinary electronic, phononic, optical, and mechanical properties.^{1–9} Well-known examples are graphene and transition-metal dichalcogenides (e.g., MoS_2).^{1–9} An essential feature of ultrathin NSs is that they are just a few atomic monolayers thick ($w \leq 2.5$ nm) but have lateral dimensions (L) of at least 100 nm. This creates a strong 1D quantum confinement, which results in unique properties.^{1–9} NSs offer compelling opportunities for fundamental studies in 2D physics and hold an immense potential for spintronic devices, field-effect transistors, nanoscale sensors, and as building blocks for batteries, photodetectors, and LEDs.^{1–9} NSs are typically obtained by exfoliation of bulk materials or grown on substrates by MBE or CVD.^{1–9} These methods are however not suitable to produce large amounts of free-standing NSs and lack control over their shape and lateral dimensions.

Solution-based “bottom-up” colloidal chemical methods offer an appealing alternative, and are emerging as promising routes to free-standing colloidal inorganic NSs, due to their versatility in terms of composition, size, shape, and surface control. Nevertheless, ultrathin colloidal NSs of inorganic semi-

conductors are still restricted to just a few materials.^{10–27} The most investigated ones are CdX ($X = \text{S}, \text{Se}, \text{Te}$) nanoplatelets ($w = 1.2\text{--}2.1$ nm; $L = 10\text{--}700$ nm, square or rectangular with irregular edges)^{10–13} and nanoribbons ($L \leq 1$ μm , tens of nm wide),^{14–17} which have been shown to possess remarkable optical properties.^{10,14,16,18–20} Ultrathin colloidal NSs of Sb_2S_3 ($w = 1.8$ nm; rectangular with ragged edges, $L = 100 \times 500$ nm),²¹ SnSe ($w = 1$ nm, $L = 300$ nm, irregularly shaped),²² PbS ($w = 2.8$ nm, square, $L \leq 1$ μm),^{23,24} ZnSe ($w = 1.4$ nm, $L = 40\text{--}160$ nm, rectangular ribbons ~ 20 nm wide),²⁵ $\beta\text{-In}_2\text{S}_3$ ($w = 0.76$ nm, $L = 22\text{--}60$ nm, hexagonal),²⁶ and $\text{Cu}_{1.96}\text{S}$ ($w = 0.65$ nm, mixed triangular and hexagonal, $L = 200$ nm)²⁷ have also been recently synthesized. Despite these recent advances, full control over the shape and dimensions of the NSs remains a challenge. Here we demonstrate a synthesis method that yields free-standing ultrathin (2 nm) Cu_{2-x}S NSs with well-defined shape (triangular or hexagonal) and sizes tunable from 100 nm to 3 μm . Moreover, these NSs do not easily fold or entangle themselves, and readily self-assemble into ordered

Received: October 24, 2014

Revised: December 2, 2014

Published: December 4, 2014

stacks. The key feature of our approach is the use of a synergistic interaction between halides (Br or Cl) and copper-thiolate metal–organic frameworks to create a template that imposes 2D constraints on the Cu-catalyzed C–S thermolysis, resulting in nucleation and growth of colloidal Cu_{2-x}S NSs.

Cu_{2-x}S is a direct p-type semiconductor with a band gap that depends on its stoichiometry (1.1–1.4 eV for $x = 0$ –0.04; 1.5 eV for $x = 0.2$; 2.0 eV for $x = 1$).²⁸ The combination of a suitable band gap, high absorption coefficient, low cost, and low toxicity has made Cu_{2-x}S a prime candidate for the large scale deployment of photovoltaics.^{28,29} Moreover, copper chalcogenide nanocrystals (NCs) have been shown to possess the unique property of holding quantum confined excitons and highly tunable localized surface plasmons on demand, opening up the way to create coupled plasmon excitons in the same NC.^{30–32} This creates a number of exciting possibilities, such as ultrafast optical switching or plasmon-enhanced photovoltaics.³⁰ Cu_{2-x}S NCs also hold promise for biomedical applications³³ and as electrodes for Li-ion batteries.²⁸ The availability of ultrathin size- and shape-controlled colloidal Cu_{2-x}S NSs may thus prove beneficial for a number of fundamental studies and potential applications. Furthermore, monovalent copper cations have a high solid state mobility due to their small size and low charge, and are therefore easily exchanged by other cations via topotactic place exchange reactions, which allow the shape and size of the parent NC to be preserved in the product NC.^{34,35} This has made copper chalcogenide NCs a versatile nanoscale template for the preparation of NCs that cannot be synthesized by direct routes.^{34,35} In the present work, we demonstrate the potential of topotactic cation exchange reactions to postsynthetically tailor the composition of the ultrathin colloidal Cu_{2-x}S NSs by converting them into ZnS and CdS, while preserving their well-defined shape, lateral dimensions, and thickness.

EXPERIMENTAL SECTION

Materials. Copper(I) acetate ($\text{Cu}(\text{OAc})$, 97%), tin(IV) tetrabromide (SnBr_4 , 99%), tin(II) dibromide (SnBr_2), tin(IV) tetrachloride pentahydrate ($\text{SnCl}_4 \cdot 5\text{H}_2\text{O}$, 98%), tin(IV) acetate ($\text{Sn}(\text{OAc})_4$), copper(I) chloride (CuCl , 97%), copper(I) bromide (CuBr , 98%), copper(I) iodide (CuI , 98%), sodium bromide (NaBr , $\geq 99\%$), sodium chloride (NaCl , 99.999%), potassium iodide (KI , 99.99%), cadmium nitrate tetrahydrate ($\text{Cd}(\text{NO}_3)_2$, 98%), zinc chloride (ZnCl_2 , reagent grade, $\geq 98\%$), tributylphosphine (TBP, 97%), trioctylphosphine (TOP, 90%), 1-dodecanethiol (DDT, $\geq 98\%$), 1-octadecene (ODE, tech., 90%), trioctylphosphine oxide (TOPO, 99%), anhydrous toluene, methanol (MeOH), and butanol (BuOH) were purchased from Sigma-Aldrich. Sulfur powder was obtained from Strem Chemicals. All chemicals were used without any further purification, except for ODE and TOPO, which were degassed at 120 °C for 2 h prior to synthesis.

Synthesis of Ultrathin Cu_{2-x}S Nanosheets. The method developed here to synthesize Cu_{2-x}S NSs is based on a synthesis protocol reported in the literature,³⁶ which was modified by adding SnBr_4 (or SnCl_4) to the reaction mixture. Typically, 27.3 mg (0.22 mmol) of $\text{Cu}(\text{OAc})$, 32.85 mg (0.075 mmol) of SnBr_4 , and 0.55 g (1.42 mmol) of TOPO were dispersed in 12.5 mL of ODE. This mixture was degassed for 30 min at 100 °C, and subsequently heated to 160 °C. At this temperature, 0.5 mL (2.1 mmol) of DDT was swiftly injected. The solution was then purged with N_2 and further heated to 220 °C. The reaction was maintained at this temperature for 40 min. Aliquots were extracted during the synthesis in order to monitor the evolution of the reaction. The Cu_{2-x}S NSs were precipitated by adding a methanol:butanol mixture and centrifuging at 3000 rpm for 15 min. Afterward, the NSs were redispersed in toluene. These washing steps were repeated three times.

Cation Exchange. The Cu^+ for Cd^{2+} or Zn^{2+} cation exchange in Cu_{2-x}S NSs was performed by using a modification of the method described by Son et al.³⁷ The metal salts that were used were $\text{Cd}(\text{NO}_3)_2$ and ZnCl_2 , which were chosen due to the relatively weak bond between the cation and anion, ensuring availability of the cations. A 0.14 mmol portion of metal salt was dissolved in 1 mL of MeOH in the presence of a small amount of TBP (100 μL). The NS solution was diluted by adding 2 mL of toluene to 1 mL of NS solution. The $\text{M}^{2+}/\text{Cu}^+$ molar ratio in the reaction mixture was ~ 3 . This ratio is a lower limit estimate, since it assumes a 100% yield and no purification losses in the synthesis of the Cu_{2-x}S NSs. After addition of the cation precursor in MeOH, the solution was stirred vigorously for several days at room temperature. The cation exchanged NSs were precipitated by adding 1:1 MeOH:BuOH, isolated by centrifugation at 3000 rpm (10 min), and redispersed in ~ 2 mL of toluene.

Characterization. Samples for optical measurements (absorption, PL, PL excitation, and PL decay curves) were prepared by directly dissolving the crude reaction mixture in anhydrous toluene under nitrogen and stored in sealed cuvettes. Samples were also analyzed by (scanning) transmission electron microscopy ((S)TEM), energy dispersive X-ray spectroscopy (EDS), electron diffraction (ED), and X-ray diffraction (XRD). Details regarding the characterization of the samples are provided in the Methods section of the Supporting Information.

RESULTS AND DISCUSSION

Solution Synthesis of Ultrathin Colloidal Cu_{2-x}S Nanosheets with Well-Defined Size and Shape. Figure 1 shows that SnBr_4 has a dramatic impact on the morphology and dimensions of colloidal Cu_{2-x}S nanocrystals (NCs) produced by hot-injection of 1-dodecanethiol (DDT) into a solution of cuprous acetate and trioctylphosphine oxide (TOPO) in octadecene (ODE), inducing the formation of ultrathin hexagonal Cu_{2-x}S nanosheets (NSs, 2 nm thick, 110 nm lateral size, Figure 1b,c). In the absence of SnBr_4 , nearly spherical Cu_{2-x}S NCs (9 nm diameter) are obtained (Figure 1a). Owing to their uniformity in thickness, the NSs readily self-assemble into ordered stacks (Figure 1c) that give rise to a series of low-

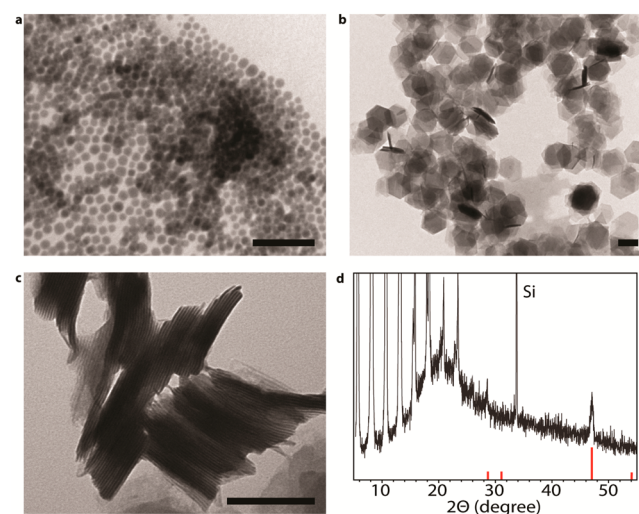


Figure 1. Transmission electron microscopy (TEM) images of colloidal Cu_{2-x}S nanocrystals synthesized in the absence (a) and in the presence (b, c) of SnBr_4 , under otherwise identical conditions. Scale bars correspond to 100 nm. (d) XRD pattern of a sample of Cu_{2-x}S nanosheets similar to those shown in (b, c), which was deposited from a toluene solution on a silicon substrate (see also Figure S1, Supporting Information). The XRD pattern of digenite (JCPDS card no. [47-1748]) is shown as a reference (red lines).

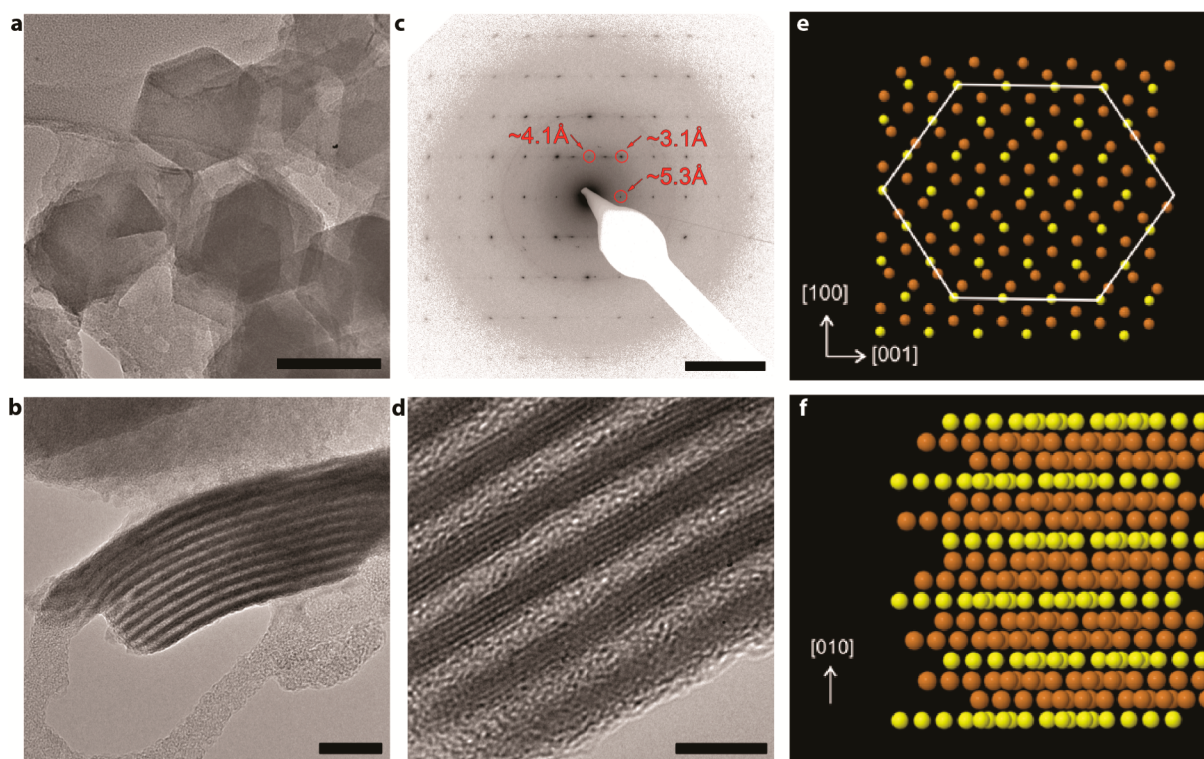


Figure 2. TEM characterization of ultrathin colloidal Cu_{2-x}S nanosheets (NSs). (a) Overview of NSs lying flat on the TEM grid (scale bar: 100 nm). (b) Side view of a NS stack, highlighting the uniformity of both the NS thickness and the inter-NS separation (scale bar: 20 nm). (c) Diffraction pattern (DP) taken from a single NS (scale bar: 5.0 nm^{-1}). (d) High-resolution TEM image (scale bar: 5 nm), showing the detail of the stack presented in part b. The crystallinity of the NSs is clearly observed in this projection. (e, f) Atomic model of the tetragonal Cu_2S structure. The brown and yellow spheres depict Cu and S atoms, respectively (see also the Supporting Discussion in the Supporting Information). (e) Projection along the b -axis of the tetragonal structure. The tetragonal a and c axes are indicated. It now becomes clear why the outer morphology of the NSs can be hexagonal, whereas the crystal structure is tetragonal. (f) Perspective view of the atomic structure with the b axis pointing upward. The buckled Cu layers are visible, corresponding to the atomic layers with dark contrast in the HRTEM image shown in part d.

angle XRD peaks (Figure 1d and Figure S1, Supporting Information), which can be ascribed to successive diffraction orders from a periodic superstructure. The peak separation (viz., $\sim 2.49^\circ$) corresponds to a periodicity of $\sim 36.7 \text{ \AA}$, indicating that the stacks consist of 2 nm thick Cu_{2-x}S nanosheets separated by one DDT monolayer (the length of a fully extended DDT molecule is 17.7 \AA , including the thiol headgroup³⁸). This is corroborated by HRTEM images, which show $\sim 2.0 \text{ nm}$ thick NSs separated by $\sim 1.6 \text{ nm}$ (Figure 2b,d). The fact that the inter-NS separation is similar to the length of one DDT molecule implies that the capping monolayers of neighboring NSs fully interpenetrate each other. This is consistent with the results reported by Pileni and co-workers for alkanethiol capped Ag and Ag_2S nanocrystals,³⁸ where alkyl chains on adjacent nanocrystals were observed to fully interdigitate for chain lengths equal to or longer than C_{12} .

The crystallinity of the nanosheets is clearly evident in the XRD pattern (Figure 1d), in the HRTEM images (Figure 2d), and in the electron diffraction (ED) patterns (Figure 2c). The binary Cu–S system has a very rich phase diagram,³⁹ and therefore, Cu_{2-x}S can crystallize in various equilibrium crystal structures (viz., monoclinic low-chalcocite Cu_2S , djurleite $\text{Cu}_{1.96}\text{S}$ and roxbyite $\text{Cu}_{1.78}\text{S}$, hexagonal high-chalcocite Cu_2S , digenite $\text{Cu}_{1.8}\text{S}$, and covellite CuS , orthorhombic djurleite $\text{Cu}_{1.96}\text{S}$ and anilite $\text{Cu}_{1.75}\text{S}$).^{39,40} These crystal structures are characterized by either hexagonal or cubic close-packing of S atoms, with Cu atoms positioned at the interstices. Transformations involving rearrangement of S atoms from cubic to

hexagonal (and vice versa) are extremely slow, leading to a number of metastable phases (e.g., low-digenite $\text{Cu}_{1.8}\text{S}$ and tetragonal Cu_{2-x}S with $x = 0.03\text{--}0.15$).³⁹

The XRD pattern in Figure 1d also shows a peak at higher angles (47°), which corresponds to a lattice spacing of 2.0 \AA . This peak may be assigned to the (1 0 20) reflection of the hexagonal digenite crystal structure (see reference XRD pattern in Figure 1d). However, the ED patterns obtained from single, flat lying NSs are not hexagonal but tetragonal (Figure 2c). Moreover, HRTEM images of stacks of NSs in a side projection (Figure 2d) reveal an interlayer distance of approximately $3.9 \pm 0.2 \text{ \AA}$. From a comparison of the experimental structural data (XRD, HRTEM, and ED) with the phase diagram of Cu_{2-x}S ,³⁹ we infer that the crystal structure of the NSs is likely the metastable tetragonal Cu_{2-x}S phase, with approximate lattice parameters $a = b = 4.0 \text{ \AA}$, $c = 11.0 \text{ \AA}$ (Figure 2e,f and Figure S2 and Supporting Discussion, Supporting Information). Assuming this structure, the spots observed in the ED pattern (Figure 2c) can be assigned to the (100) and (002) lattice spacings, with the a and c axes lying in the plane of the NS and the b axis perpendicular to it. The a and b axes are equivalent and could be interchanged. The interlayer distance observed in the HRTEM images (Figure 2d) can then be taken to correspond to the 4.0 \AA spacing between the buckled Cu atomic layers along the b -axis in the tetragonal Cu_{2-x}S crystal structure (Figure 2e,f and Supporting Discussion, Supporting Information). This analysis indicates that the peak observed in the XRD pattern (Figure 1d) actually corresponds to the (200) reflection

of a metastable tetragonal polymorph of digenite. We suggest the tetragonal phase as the most plausible crystal structure, as the beam sensitivity of the sample prohibits a profound determination of the crystal structure.

Energy-dispersive X-ray spectroscopy (EDS) was used to analyze the sample, confirming that the NSs are made of Cu_{2-x}S (Figure S3, Supporting Information). Intriguingly, the NSs also contain a significant amount of Br but are devoid of Sn (average Cu:S:Sn:Br elemental ratios are $2.0 \pm 0.2:1.0:0:0.30 \pm 0.06$), even if the nanocrystals are taken directly from the diluted crude reaction mixture and analyzed without any washing. This implies that Sn and Br play very different roles in the formation of ultrathin Cu_{2-x}S NSs, despite their common origin (i.e., SnBr_4).

Unraveling the Roles of Br, Sn, and DDT. To clarify the influence of the different components of the reaction system, a series of control experiments was carried out. The results are summarized in Figure 3 and in the Supporting Information

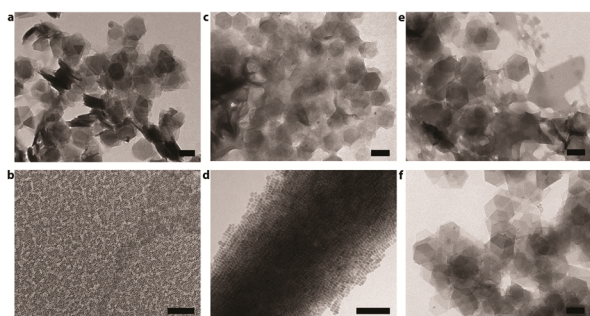


Figure 3. TEM images of colloidal Cu_{2-x}S NCs obtained with different additives. The composition of the reaction medium and reaction conditions are identical in all cases, except for the additive. Scale bars correspond to 100 nm. (a) SnBr_4 . (b) $\text{Sn}(\text{acetate})_4$. (c) SnBr_4 , but its concentration is $1/2$ of that used in part a. (d) SnBr_4 , but its concentration is $1/4$ of that used in part a. (e) No additive, but $\text{Cu}(\text{acetate})$ is replaced by CuBr . (f) NaBr as additive and CuBr instead of $\text{Cu}(\text{acetate})$.

(Table S1). As shown above (Figures 1 and 2) and in Figure 3a, ultrathin hexagonal Cu_{2-x}S NSs are obtained if SnBr_4 is added to a reaction system that would otherwise yield spherical Cu_{2-x}S NCs. In contrast, if $\text{Sn}(\text{acetate})_4$ is used instead of SnBr_4 , the reaction still yields small spherical NCs (Figure 3b). The use of SnBr_2 instead of SnBr_4 yields only irregularly shaped and aggregated sheets (Figure S4, Supporting Information).

The impact of SnBr_4 is clearly concentration dependent, since coexisting hexagonal NSs and irregularly shaped thin materials are obtained if the concentration of SnBr_4 is halved (Figure 3c and Figure S5, Supporting Information). Interestingly, the elemental composition of the irregularly shaped thin material significantly differs from that of the hexagonal NSs (Cu:S:Br ratios are $1.41 \pm 0.14:1.0:0.03 \pm 0.01$ and $2.0 \pm 0.2:1.0:0.30 \pm 0.06$, respectively; Figure S5, Supporting Information). If the concentration of SnBr_4 is further reduced to a quarter of that originally used, nanosheets are no longer formed, but instead small Cu_{2-x}S nanodisks (aspect ratio ~ 2) are obtained (Figure 3d), which readily self-assemble into corn cob superlattices (Figure S6, Supporting Information). Coexisting hexagonal NSs and irregularly shaped thin materials are also obtained in the absence of SnBr_4 , provided $\text{Cu}(\text{acetate})$ is replaced by CuBr (Figure 3e). Remarkably, if CuBr is used in

combination with NaBr , only well-defined ultrathin hexagonal Cu_{2-x}S NSs are obtained (Figure 3f).

These observations unambiguously demonstrate that Br plays a pivotal role in the formation of Cu_{2-x}S NSs, while Sn(IV) has only the adjuvant role of ensuring that a sufficiently high concentration of Br is readily available in solution. The failure of SnBr_2 to yield well-formed NSs (Figure S4, Supporting Information) can be attributed to the lower availability of Br, since Br (a soft Lewis base) forms a much stronger bond with Sn(II) (a soft Lewis acid) than with Sn(IV) (a hard Lewis acid). Furthermore, experiments in which dodecanethiol was replaced by other sulfur sources clearly demonstrate that well-defined Cu_{2-x}S NSs can be formed only when long chain alkanethiols (DDT and octadecanethiol) are used (Figure S7, Supporting Information). For example, phenylethanethiol (a bulky and short thiol) yields only irregularly shaped and aggregated thin material, while elemental sulfur leads to small and polydisperse nanocrystals (Figure S7, Supporting Information). In contrast, 1-octadecanethiol (ODE) yields hexagonal NSs similar to those formed using 1-DDT, except for the larger inter-NS separation in the stacks (viz., 2 nm; see the inset of Figure S7b, Supporting Information). The longer inter-NS separation is consistent with the increase in length of the alkyl chain from 1.77 to 2.5 nm from 1-DDT to 1-ODE, which also results in a higher incidence of gauche defects near the terminal methyl end of the alkyl chain.³⁸ This allows pseudorotational motion of the chain about the R–S bond axis, leading to interparticle separations that are shorter than the alkyl chain length.³⁸

Size and Shape Control. The lateral dimensions of the NSs can be increased up to ~ 400 nm, while preserving their shape, by diluting the reaction system with ODE (Figure 4a,b

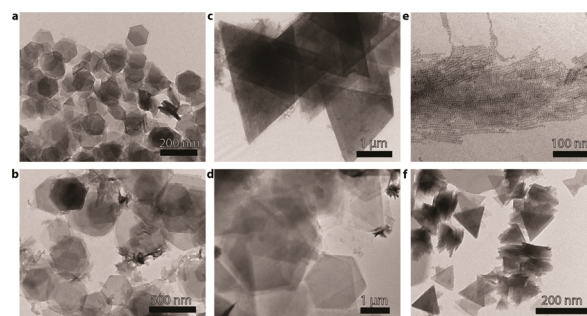


Figure 4. TEM images of colloidal Cu_{2-x}S NCs obtained under different reaction conditions. (a) 17 mM $\text{Cu}(\text{acetate})$, 5.8 mM SnBr_4 , and 0.1 M TOPO in ODE; injection of 2.1 mmol of DDT. (b) Same as part a but diluted by a factor of 4 with ODE. (c) Same as part a but without TOPO. (d) Same as part a but with the TOPO concentration reduced to 20 mM. (e) SnCl_4 instead of SnBr_4 while keeping all concentrations unchanged. (f) SnCl_4 instead of SnBr_4 but with the SnCl_4 concentration increased by a factor of 3.

and Figure S8 and Table S1, Supporting Information). The lateral dimensions of the hexagonal NSs can also be increased by decreasing the concentration of the coordinating ligand TOPO (Figure 4d), allowing the synthesis of $2 \mu\text{m}$ wide hexagonal NSs. In contrast, the total absence of TOPO changes both the lateral dimensions and shape of the NSs, yielding large ($3\text{--}4 \mu\text{m}$) triangular NSs (Figure 4c). These experiments clearly demonstrate that TOPO affects the shape of the NSs, converting them from triangular to hexagonal, while simultaneously decreasing the lateral growth rates. The thickness of the nanosheets is not affected, as confirmed by XRD measurements

(Figure S9, Supporting Information), resulting in well-defined 2 nm thick hexagonal nanosheets with aspect ratios up to 1000.

The size and shape of the NSs can also be tailored by using SnCl_4 instead of SnBr_4 , although a higher concentration of SnCl_4 is required to produce ultrathin NSs (Figure 4e,f). It is noteworthy that the use of SnCl_4 instead of SnBr_4 changes the NS shape from hexagonal to triangular. The effect is clearly due to the Cl, since a similar result is obtained by replacing Cu(acetate) and SnCl_4 by CuCl and NaCl, respectively, in the absence of any other additive (Figure S10 and Table S1, Supporting Information). The fact that a higher concentration of SnCl_4 is needed to form NSs can be ascribed to the lower Cl availability due to the stronger Sn–Cl bond.

Interestingly, ultrathin NSs are not obtained if CuCl and NaCl are replaced by CuI and KI, respectively. Instead, this reaction yields a (seemingly) 3D porous network of interconnected particles (Figure S11, Supporting Information). The differences between the effect of different halides (X) can be tentatively ascribed to changes in the Cu–X bond strength. Since Cu(I) is a very soft Lewis acid, the Cu–X bond should become stronger in the sequence $\text{Cl} < \text{Br} < \text{I}$, as a result of the increase in the soft character of the halides as Lewis bases. This point will be discussed in more detail in the mechanism section below.

Formation Mechanism. Several mechanisms have been proposed for the formation of ultrathin colloidal NSs of semiconductors: 2D oriented attachment of PbS NCs,²³ self-assembly of $(\text{CdX})_n$ (X = S, Se) magic-size clusters (MSCs) within 2D lamellar templates,^{14–17} 2D growth by monomer addition to $(\text{CdX})_n$ MSC seeds,^{10,11} and 2D-constrained growth of CdSe nanodisks within soft templates formed by close-packed fatty acid layers.¹² It is interesting to note that recent work by Buhro and co-workers has provided compelling evidence that the formation of PbS nanosheets by 2D oriented attachment of small PbS nanoparticles is directed by lamellar-mesophase templates.²⁴ A soft-template mechanism has also been proposed to explain the formation of slightly thicker ($w = 3.2$ nm) covellite CuS nanosheets.⁴¹ To investigate whether a soft template mechanism is also involved in the formation of the ultrathin Cu_{2-x}S NSs reported in the present work, we followed the evolution of the reaction by TEM and optical spectroscopy.

Directly after DDT injection, irregularly shaped thin sheets form (Figure 5a). As the reaction progresses, the irregular thin

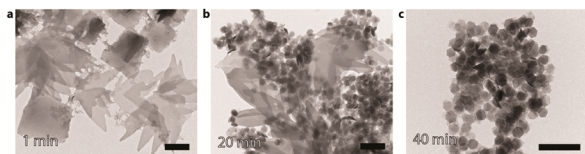


Figure 5. TEM images of samples collected at different time points after the injection of DDT into a solution of Cu(I) acetate, SnBr_4 , and TOPO in ODE at 220 °C (scale bars correspond to 500 nm).

sheets gradually disappear, while hexagonal Cu_{2-x}S NSs form and increase in concentration, eventually becoming the only nanostructure present (Figure 5). The temporal evolution observed in Figure 5 bears similarities with that previously reported for the reaction between Cu(I) salts and DDT in solution at high temperatures (185–220 °C),^{36,42} where irregularly shaped thin sheets are also observed at early reaction times and gradually disappear as Cu_{2-x}S NCs are

formed.^{36,42} Nevertheless, in these cases, ultrathin NSs are not formed, but instead, the reaction yields either spherical NCs (5–18 nm)^{36,42} or small nanodisks (9 by 13–17 nm),³⁶ in striking contrast with the present results. This difference is remarkable, and is clearly due to the presence of tin tetrahalides. Tin(IV) compounds (viz., SnCl_4 and $\text{Sn}(\text{acetylacetonate})_2\text{Cl}_2$) have been previously shown to affect the shape of Cu_{2-x}S NCs obtained by reacting Cu(II)-acetylacetonate and neat DDT, leading to the formation of either aggregated ultrathin $\text{Cu}_{1.96}\text{S}$ NSs ($w = 0.65$ nm, $L = 200$ nm, hexagonal or triangular without shape selectivity)²⁷ or Cu_{2-x}S nanodisks ($w = 3.2$ –6 nm; $L = 13$ –84 nm),⁴³ under conditions that would otherwise yield spherical NCs. This has been tentatively ascribed to *in situ* generated $[\text{Sn}_x\text{S}_y]$ species (e.g., $[\text{Sn}_2\text{S}_6]^{4-}$),^{27,43} but the results presented above unambiguously demonstrate that the effect is actually due to the halides and that Sn(IV) is important only to the extent that it ensures the availability of sufficiently high halide concentrations in the growth solution. It is also clear that the formation of ultrathin Cu_{2-x}S NSs results from a synergistic interaction between halides and Cu-alkanethiolate complexes that are formed *in situ*, since the use of sulfur sources other than alkanethiols does not yield nanosheets (see above and Figure S7, Supporting Information).

Copper-thiolates have been extensively used as single source precursors to produce Cu_{2-x}S NCs, both by solventless and solution based routes.^{36,40,42–46} These synthetic protocols have yielded a wealth of different nanocrystal morphologies (quasi-spheres, hexagonal bipyramids and bifrustums, hexagonal nanodisks, and nanoplatelets),^{36,40,42–46} but ultrathin nanosheets are rare, and have been observed only when halides were present in the reaction medium (e.g., ref 27 and the present work). The reaction mechanisms are not yet well understood, although a recent *in situ* synchrotron powder X-ray diffraction study has demonstrated that the C–S bond cleavage is the limiting step in the formation and growth of colloidal Cu_{2-x}S NCs by thermolysis of $[\text{Cu}(\text{DDT})]$ in solution.⁴⁴ Cu-alkanethiolates form a metal–organic framework (MOF) that is stable as a lamellar solid up to 143.5 °C (for Cu-DDT), when it undergoes a phase transition to a mesogenic liquid crystal.⁴⁷ The structure of this liquid crystal phase is particularly relevant for the present discussion, as it consists of a hierarchically self-assembled hexagonal columnar mesophase, in which each column is made of a stack of tetranuclear $[\text{Cu}_4(\text{DDT})_4]$ disks that are kept together by weaker Cu–S interdisk interactions (Figure S12, Supporting Information). The irregularly shaped sheets observed at early reaction stages in this and other works^{36,42} can thus be tentatively ascribed to intact Cu-thiolate frameworks. However, the intercolumn and interdisk interactions break at sufficiently high temperatures (e.g., 205.6 °C for neat Cu-DDT), leading to an isotropic liquid (Figure S12, Supporting Information),⁴⁷ which, upon further heating, will undergo Cu-catalyzed C–S thermolysis, producing independent $[\text{Cu}_4\text{S}_4]$ nuclei that further grow into quasi-spherical NCs or hexagonal nanodisks by monomer addition.^{36,42} The different fate of the irregular sheets in the present work suggests that halides have a stabilizing effect on the Cu-thiolate framework, preserving its 2D-structural integrity at temperatures that are sufficiently high to sustain C–S thermolysis. Interestingly, recent work by Tao and co-workers has demonstrated that the ordered liquid crystalline mesophase plays an essential role in templating the nanocrystal morphology obtained by solventless thermolysis of Cu-

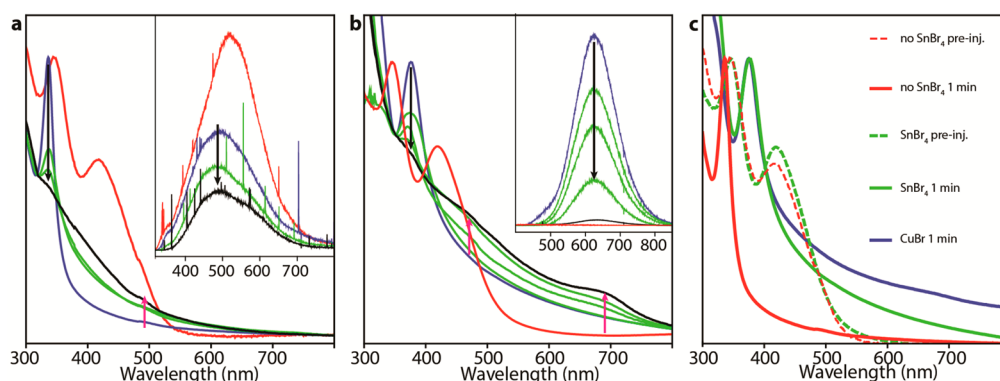


Figure 6. (a, b) Temporal evolution of the absorption and PL (insets) spectra of samples collected at different time points during Cu_{2-x}S NC syntheses performed without (a) and with SnBr_4 (b). The reaction conditions and composition of the reaction mixture were identical in both cases, except for the presence or absence of SnBr_4 . Red and blue lines give, respectively, the spectra prior to and 1 min after DDT injection. Black lines correspond to the final samples, collected at 15 min for part a (9 nm Cu_{2-x}S NCs) and 80 min for part b (ultrathin hexagonal Cu_{2-x}S NSs). Intermediate time points are given by green lines (4 and 10 min in part a; 4, 15, and 33 min in part b). The PL excitation spectrum and PL decay curve of the Br-modified Cu-thiolate precursor complex are shown in Figure S14 (Supporting Information). The arrows indicate the evolution of the peak intensities, and show that Cu-thiolate (black arrow) is consumed as Cu_{2-x}S (purple arrow) forms. (c) Comparison of the absorption of samples collected prior to and 1 min after injection.

thiolates, so that hexagonal Cu_{2-x}S nanodisks and nanoplatelets are only obtained for Cu-thiolates that adopt an inverse columnar mesophase at the reaction temperature.⁴⁵ It is thus likely that the 2D-constrained growth observed in the present work is due to a templating framework formed by halides and the Cu-thiolate MOF.

Our experiments show that halides have a dramatic impact on both the optical spectra and the morphology of the Cu-thiolate precursor complexes formed upon heating of a mixture of Cu(I) salts and 1-DDT in ODE to 190 °C (Figure S13, Supporting Information). This temperature is just below the onset of C–S thermolysis, and therefore also below the nucleation threshold. The results presented in Figure S13 (Supporting Information) thus reflect the properties of the precursor complexes formed in the reaction mixture. The presence of Br clearly affects the morphology of the Cu-thiolate precursor complex at room temperature, converting it from a 3D gel network (Figure S13a, Supporting Information) to irregularly shaped thin sheets (Figure S13b, Supporting Information). A 3D Cu-DDT gel has been observed before by Han and co-workers,⁴² by cooling a solution of Cu-DDT in DDT from 200 °C to room temperature. It is interesting to note that this implies that the Cu-thiolate lamellar structure does not form under these conditions, suggesting that the intercolumn van der Waals interactions are weakened by the presence of the solvent molecules (ODE or DDT). The interdisk Cu–S interactions are however sufficiently strong to keep the columns intact, allowing the formation of a 3D gel network of interconnected strings. The observation of 2D sheets in the presence of Br (Figure S13b, Supporting Information) can thus be interpreted as evidence that the intercolumn interaction is reinforced by halides, allowing the formation of lamellar frameworks.

Halides may be expected to have a large impact on MOFs based on Cu(I) as connectors, since they are capable of binding as polycoordinated bridging atoms between multiple (up to 4) Cu(I) atoms, often forming $[(\text{CuX})\text{L}]_n$ (L = sulfur-donor ligand) coordination polymers with highly variable structures, ranging from 1D to 3D.⁴⁹ As will be discussed below, the pronounced changes observed in the optical spectra of the precursor complexes in the presence of halides (Figure 6 and

Figures S13d and S14, Supporting Information) clearly demonstrate the formation of direct bonds between halides and Cu(I) atoms in the Cu-thiolate complexes. The differences between the morphology of the Cu_{2-x}S NCs obtained in the presence of chloride and bromide (ultrathin nanosheets, Figures 1–4) and iodide (porous network of interconnected particles, Figure S11, Supporting Information) suggest that the resulting halide-Cu-thiolate MOFs have different geometries (2D for Cl and Br, 3D for I). This can be rationalized in terms of the different strengths of the Cu–X (X = Cl, Br, I) interactions, which are the strongest for Cu–I, rendering the geometry of (CuI)L coordination polymers dramatically different from those of (CuBr)L and (CuCl)L.⁴⁹

Optical spectroscopy is thus particularly useful to unravel the role of the halides, since it allows the formation of Cu_{2-x}S NCs to be followed, while simultaneously signaling the presence of precursors and intermediate reaction compounds. The optical spectra of samples collected during the synthesis (Figure 6 and Figure S14, Supporting Information) clearly show that halides have no effect on the identity of the complexes present prior to DDT injection but dramatically affect the electronic structure of the Cu-thiolate complex formed immediately after the injection (Figure 6c). When no halides are added, an absorption transition is observed at 325 nm (Figure 6a), while in the presence of Br this absorption transition shifts to 375 nm (Figure 6b). We note that these spectra are identical to those obtained by heating up the reaction mixture to 190 °C (Figure S13d, Supporting Information), indicating that the same precursor complexes are formed. The photoluminescence (PL) of the Cu-thiolate precursor complexes also changes dramatically upon addition of halides (Figure 6a,b and Figure S14, Supporting Information). It is evident that these precursor complexes are consumed as the reaction progresses, since both the absorption and PL peaks associated with them decrease, while the characteristic absorption of Cu_{2-x}S increases (Figure 6a,b). This is consistent with the TEM observations discussed above (Figure 5).

The optical properties of the precursor complexes formed upon DDT injection are typical of polynuclear Cu(I) complexes with halides and sulfur-donor ligands.^{48,49} Multi-nuclear Cu(I) complexes with sulfur or halide donors typically

show efficient PL at room temperature, peaking at wavelengths ranging from 500 to 700 nm, depending on the ligands and the structure of the complex or coordination polymer.⁴⁸ The PL is often characterized by two independent bands, where the high energy PL peak originates from a Cu/halide-to-ligand charge transfer triplet state and the low energy PL peak originates from a Cu_4X_4 ($\text{X} = \text{donor atom, i.e., sulfur or halide}$) centered triplet state, which is a combination of X to Cu(I) charge transfer and d–s transitions.⁴⁸ The low energy PL has larger Stokes shifts and longer lifetimes than the high energy PL. Moreover, the quantum yield of the high energy PL is lower, making it often absent at room temperature. The peak position, Stokes shift (viz., 1.3 eV), and lifetime (viz., 7.8 μs with a faster initial component of 1.8 μs ; Figure S14, Supporting Information) observed for the Br-modified Cu-thiolate precursor complex are consistent with emission from the low energy state (i.e., the Cu_4X_4 centered triplet state). The large shifts induced in both the absorption and PL spectra by the presence of Br (viz., 0.34 and 0.48 eV, respectively) and the increase in the Stokes shift (from 1.17 to 1.3 eV) thus provide compelling evidence that Br atoms coordinate directly to Cu(I) atoms in the Cu-DDT precursor complexes. This is further supported by the dramatic increase observed in the PL QY in the presence of Br, since shorter Cu–Cu distances are known to lead to more efficient PL at RT.⁴⁸ It should be noted that the optical spectra provide no signatures of MSCs or stepwise growth,^{50,51} thereby excluding mechanisms involving MSCs.

We propose that in the present case binding between halides (Br or Cl) and Cu(I) atoms in the Cu-thiolate precursor complexes leads to the formation of a soft 2D template that remains structurally intact beyond the onset of the C–S bond thermolysis. The thermally induced C–S bond cleavage is catalyzed by the Cu(I) atoms,⁵² and therefore, only DDT molecules directly involved in the Cu-thiolate framework will undergo thermolysis. Since the C–S bond cleavage is the limiting step in the formation of colloidal Cu_{2-x}S NCs by thermolysis of $[\text{Cu}(\text{DDT})]$ in solution,⁴⁴ the soft template will impose 2D constraints on the nucleation and growth of the Cu_{2-x}S NCs, thereby leading to the formation of ultrathin colloidal Cu_{2-x}S nanosheets. This mechanism is analogous to the nucleation and growth of colloidal NCs in solution,⁵³ except for the fact that it is two-dimensionally constrained. The impact of TOPO and of the overall concentration of the reaction system on the lateral dimensions and shape of the NSs can easily be understood from this perspective, since coordinating ligands are well-known to modulate the growth rates of colloidal NCs by competing with the monomers (i.e., $[\text{CuS}]$ units) for the binding sites, in a strongly facet-dependent fashion.⁵³ It is thus likely that both the final shape and the crystal structure of the NSs are determined by the interplay between the constraints imposed by the 2D soft template, the C–S thermolysis rates, and coordination by TOPO, halides, and intact DDT molecules. It is interesting to note that the mechanism unraveled in the present work may be applicable also to the preparation of ultrathin 2D nanocrystals of other compositions, since lamellar metal thiolate complexes are widely used as single source precursors in the synthesis of nanocrystals of a variety of transition metal sulfides (e.g., FeS, Ni_3S_4 , Cu_{2-x}S , Co_9S_8 , CdS, ZnS, PdS, Ag_2S , PbS, and Bi_2S_3).^{54–60} In this context, it is worth noting that recent work has demonstrated that Ni_9S_8 can exhibit 2D growth, yielding colloidal nanocrosses, when nickel thiolate is used as a single source precursor, provided halide ions are present in the

reaction medium.⁶¹ In the absence of halides, only short nanorods are obtained. Although the authors of ref 61 suggest a different mechanism to account for these observations (viz., halides would reduce the formation rate of nickel thiolate, thereby inhibiting nucleation and slowing down the growth kinetics, and, as a result, promoting 2D growth),⁶¹ we argue that templating by a 2D halide-Ni-thiolate MOF is also a plausible mechanism.

Composition Tailoring by Cation Exchange. Nanoscale cation exchange (CE) provides a versatile strategy for synthesizing colloidal NCs with compositions and morphologies that are not accessible by conventional methods.^{34,35,51,62–68} Very often, the anionic sublattice is not affected by the cation exchange, leading to a topotactic reaction, through which the size and shape of the parent NCs are preserved in the product NCs, despite the compositional change.^{34,62} Interestingly, the degree of cation exchange can be controlled, leading to partial or total replacement of the native cation.^{34,62} In the case of partial exchange, the elemental profile distribution within the product NC can also be controlled, so that core/shell heteronanocrystals,^{65,66} homogeneous or gradient alloy nanocrystals,⁶⁶ and doped nanocrystals^{67,68} can be obtained, depending on the chemical system and reaction conditions.^{34,62,65–67} Topotactic CE reactions in which Cu^+ is exchanged for other cations have been extensively investigated in copper chalcogenides, yielding NCs with metastable shapes and structures that would otherwise not be attainable.^{34,35,62–64}

In the present work, CE reactions were exploited to convert Cu_{2-x}S NSs into CdS and ZnS NSs (Figure 7). The results

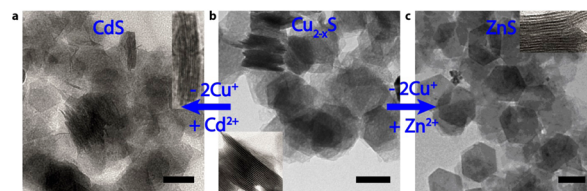


Figure 7. TEM images of ultrathin colloidal nanosheets (NSs) of various compositions (insets show stacks of NSs): (a) NSs obtained after Cu^+ for Cd^{2+} exchange in Cu_{2-x}S NSs (ratio Cd:S:Cu:Br = $0.90 \pm 0.04:1.0:0.06 \pm 0.01:0.03 \pm 0.01$); (b) Cu_{2-x}S NSs used as parent NCs for the NSs shown in parts a and c (ratio S:Cu:Br = $1.0:2.0 \pm 0.2:0.30 \pm 0.06$); (c) NSs obtained after Cu^+ for Zn^{2+} exchange in Cu_{2-x}S NSs (ratio Zn:S:Cu:Br = $0.97 \pm 0.04:1.0:0.30 \pm 0.06:0.10 \pm 0.02$).

show that the Cu^+ for Cd^{2+} or Zn^{2+} exchange reactions in Cu_{2-x}S NSs are topotactic, thereby preserving the shape and size (both lateral dimensions and thickness) of the parent NSs in the product NSs. This is remarkable considering the ultrathin dimensions of the parent NSs, and implies that the sulfide anionic framework is very robust and can readily accommodate and relax the local strain induced by the exchange of two Cu^+ ions by one Cd^{2+} or Zn^{2+} cation. This is in line with the crystal structure proposed for the Cu_{2-x}S NSs (Figure 2e,f, and Supporting Discussion, Supporting Information). The cation exchange did not reach completion, yielding Cu-doped CdS NSs and ZnS NSs. The doping level in the CdS NSs is sufficiently low to allow observation of efficient PL associated with exciton recombination in the Cu^+ dopants⁶⁹ (Figure S15, Supporting Information). These results demonstrate that the Cu_{2-x}S NSs developed here can be used as well-defined

morphological templates for the preparation of compositionally diverse NSs, thus allowing access to a whole range of novel ultrathin colloidal NSs that cannot be synthesized by direct routes.

CONCLUSIONS

The novel “bottom-up” solution-based synthesis method developed in this work yields 2 nm thick colloidal Cu_{2-x}S NSs with well-defined size and shape (hexagonal or triangular). The lateral dimensions of these ultrathin NSs can be tuned from 100 nm to 3 μm . These NSs are very robust and do not easily fold or aggregate, and therefore offer excellent solution processability. They can also be used as building blocks for self-organized superstructures. Moreover, we demonstrate that the composition of the NSs can be postsynthetically tailored by exploiting topotactic cation exchange reactions, while preserving their well-defined shape, lateral dimensions, and thickness. The method presented here thus holds great promise as a route to solution-processable compositionally diverse ultrathin colloidal NSs with well-defined shape and size. It should be noted that combined control over surface, size, shape, and composition can be used to modify the properties of the NSs or to bestow them with novel functionalities, paving the way toward tailor-made NSs.

ASSOCIATED CONTENT

Supporting Information

Additional details on the characterization methods, discussion on the crystal structure of tetragonal Cu_{2-x}S , low-angle XRD patterns of two different samples of Cu_{2-x}S nanosheets, elemental mapping of a selected nanosheet, table summarizing the outcome of all the control syntheses, TEM images of samples prepared under various different conditions, optical data (absorption, PL, and PLE spectra and PL decay curves) of samples collected immediately after the injection of DDT into the reaction mixture, and optical spectra (absorption, PL, and PLE) of Cu-doped ultrathin CdS nanosheets. This material is available free of charge via the Internet at <http://pubs.acs.org>.

AUTHOR INFORMATION

Corresponding Author

*E-mail: c.demello-donega@uu.nl

Notes

The authors declare no competing financial interest.

ACKNOWLEDGMENTS

W.v.d.S. and C.d.M.D. acknowledge financial support from the division of Chemical Sciences (CW) of The Netherlands Organization for Scientific Research (NWO) under Grant No. ECHO.712.012.001. The authors are grateful to Johannes D. Meeldijk (Utrecht University) for his assistance regarding TEM-EDS measurements. X.K. and S.B. acknowledge funding from the European Research Council under the Seventh Framework Program (FP7) ERC Grant No. 246791—COUNTATOMS and ERC Grant No. 335078-COLOURATOM. Financial support from the EU FP7-Integrated Infrastructure Initiative-I3 program ESTEEM2(312483) is gratefully acknowledged.

REFERENCES

- (1) Butler, S. Z.; Hollen, S. M.; Cao, L.; Cui, Y.; Gupta, J. A.; Gutie, H. R.; Heinz, T. F.; Hong, S. S.; Huang, J.; Ismach, A. F.; et al. *ACS Nano* **2013**, *7*, 2898–2926.
- (2) Wang, Q. H.; Kalantar-Zadeh, K.; Kis, A.; Coleman, J. N.; Strano, M. S. *Nat. Nanotechnol.* **2012**, *7*, 699–712.
- (3) Xu, M.; Liang, T.; Shi, M.; Chen, H. *Chem. Rev.* **2013**, *113*, 3766–3798.
- (4) Chhowalla, M.; Shin, H. S.; Eda, G.; Li, L.-J.; Loh, K. P.; Zhang, H. *Nat. Chem.* **2013**, *5*, 263–275.
- (5) Rao, C. N. R.; Ramakrishna Matte, H. S. S.; Maitra, U. *Angew. Chem., Int. Ed.* **2013**, *52*, 13162–13185.
- (6) Rogers, J. A.; Lagally, M. G.; Nuzzo, R. G. *Nature* **2011**, *477*, 45–53.
- (7) Narita, A.; Feng, X.; Hernandez, Y.; Jensen, S. A.; Bonn, M.; Yang, H.; Verzhbitskiy, I. A.; Casiraghi, C.; Hansen, M. R.; Koch, A. H. R.; et al. *Nat. Chem.* **2014**, *6*, 126–132.
- (8) Yin, Z.; Zhu, J.; He, Q.; Cao, X.; Tan, C.; Chen, H.; Yan, Q.; Zhang, H. *Adv. Energy Mater.* **2014**, *4*, 1300574.
- (9) Huang, X.; Tan, C.; Yin, Z.; Zhang, H. *Adv. Mater.* **2014**, *26*, 2185–2204.
- (10) Bouet, C.; Tessier, M. D.; Ithurria, S.; Mahler, B.; Nadal, B.; Dubertret, B. *Chem. Mater.* **2013**, *25*, 1262–1271.
- (11) Ithurria, S.; Bousquet, G.; Dubertret, B. *J. Am. Chem. Soc.* **2011**, *133*, 3070–3077.
- (12) Li, Z.; Peng, X. *J. Am. Chem. Soc.* **2011**, *133*, 6578–6586.
- (13) Hutter, E. M.; Bladt, E.; Goris, B.; Pietra, F.; van der Bok, J. C.; Boneschanscher, M. P.; de Mello Donega, C.; Bals, S.; Vanmaekelbergh, D. *Nano Lett.* **2014**, *14*, 6257–6262.
- (14) Yang, J.; Son, J. S.; Yu, J. H.; Joo, J.; Hyeon, T. *Chem. Mater.* **2013**, *25*, 1190–1198.
- (15) Son, J. S.; Park, K.; Kwon, S. G.; Yang, J.; Choi, M. K.; Kim, J.; Yu, J. H.; Joo, J.; Hyeon, T. *Small* **2012**, *8*, 2394–2402.
- (16) Yu, J. H.; Liu, X.; Kweon, K. E.; Joo, J.; Park, J.; Ko, K.-T.; Lee, D. W.; Shen, S.; Tivakornsasithorn, K.; Son, J. S.; et al. *Nat. Mater.* **2010**, *9*, 47–53.
- (17) Liu, Y. H.; Wang, F. D.; Wang, Y. Y.; Gibbons, P. C.; Buhro, W. E. *J. Am. Chem. Soc.* **2011**, *133*, 17005–17013.
- (18) Ithurria, S.; Tessier, M. D.; Mahler, B.; Lobo, R. P. S. M.; Dubertret, B.; Efros, A. L. *Nat. Mater.* **2011**, *10*, 936–941.
- (19) Pelton, M.; Ithurria, S.; Schaller, R. D.; Dolzhenkov, D. S.; Talapin, D. V. *Nano Lett.* **2012**, *12*, 6158–6163.
- (20) Tessier, M. D.; Mahler, B.; Nadal, B.; Heuclin, H.; Pedetti, S.; Dubertret, B. *Nano Lett.* **2013**, *13*, 3321–3328.
- (21) Malakooti, R.; Cademartiri, L.; Migliori, A.; Ozin, G. A. *J. Mater. Chem.* **2008**, *18*, 66–69.
- (22) Li, L.; Chen, Z.; Hu, Y.; Wang, X.; Zhang, T.; Chen, W.; Wang, Q. *J. Am. Chem. Soc.* **2013**, *135*, 1213–1216.
- (23) Schliehe, C.; Juarez, B. H.; Pelletier, M.; Jander, S.; Greshnykh, D.; Nagel, M.; Meyer, A.; Foerster, S.; Kornowski, A.; Klinke, C.; et al. *Science* **2010**, *329*, 550–553.
- (24) Morrison, P. J.; Loomis, R. A.; Buhro, W. E. *Chem. Mater.* **2014**, *26*, 5012–5019.
- (25) Park, H.; Chung, H.; Kim, W. *Mater. Lett.* **2013**, *99*, 172–175.
- (26) Park, K. H.; Jang, K.; Son, S. U. *Angew. Chem., Int. Ed.* **2006**, *45*, 4608–4612.
- (27) Yi, L.; Gao, M. *Cryst. Growth Des.* **2011**, *11*, 1109–1116.
- (28) Zhao, Y.; Burda, C. *Energy Environ. Sci.* **2012**, *5*, 5564–5576.
- (29) Wadia, C.; Alivisatos, A. P.; Kammen, D. M. *Environ. Sci. Technol.* **2009**, *43*, 2072–2077.
- (30) Luther, J. M.; Jain, P. K.; Ewers, T.; Alivisatos, A. P. *Nat. Mater.* **2011**, *10*, 361–366.
- (31) Kriegel, I.; Jiang, C.; Rodríguez-Fernández, J.; Schaller, R. D.; Talapin, D. V.; da Como, E.; Feldmann, J. *J. Am. Chem. Soc.* **2012**, *134*, 1583–1590.
- (32) Hsu, S. W.; Ngo, C.; Tao, A. R. *Nano Lett.* **2014**, *14*, 2372–2380.
- (33) Goel, S.; Chen, F.; Cai, W. *Small* **2014**, *10*, 631–645.

- (34) Beberwyck, B. J.; Surendranath, Y.; Alivisatos, A. P. *J. Phys. Chem. C* **2013**, *117*, 19759–19770.
- (35) Li, H.; Brescia, R.; Povia, M.; Prato, M.; Bertoni, G.; Manna, L.; Moreels, I. *J. Am. Chem. Soc.* **2013**, *135*, 12270–12278.
- (36) Wang, Y.; Hu, Y.; Zhang, Q.; Ge, J.; Lu, Z.; Hou, Y.; Yin, Y. *Inorg. Chem.* **2010**, *49*, 6601–6608.
- (37) Son, D. H.; Hughes, S. M.; Yin, Y.; Alivisatos, A. P. *Science* **2004**, *306*, 1009–1012.
- (38) Pileni, M. P. *J. Phys. Chem. B* **2001**, *105*, 3358–3371.
- (39) Chakrabarti, D. J.; Laughlin, D. E. *Bull. Alloy Phase Diagrams* **1983**, *4*, 254–270.
- (40) Li, W.; Shavel, A.; Guzman, R.; Rubio-Garcia, J.; Flox, C.; Fan, J.; Cadavid, D.; Ibáñez, M.; Arbiol, J.; Morante, J. R.; Cabot, A. *Chem. Commun.* **2011**, *47*, 10332–10337.
- (41) Du, Y.; Yin, Z.; Zhu, J.; Huang, X.; Wu, X.-J.; Zeng, Z.; Yan, Q.; Zhang, H. *Nat. Commun.* **2012**, *3*, 1177.
- (42) Han, W.; Yi, L.; Zhao, N.; Tang, A.; Gao, M.; Tang, Z. *J. Am. Chem. Soc.* **2008**, *130*, 13152–13161.
- (43) Li, X.; Shen, H.; Niu, J.; Li, S.; Zhang, Y.; Wang, H.; Li, L. *J. Am. Chem. Soc.* **2010**, *132*, 12778–12779.
- (44) Noerby, P.; Johnsen, S.; Iversen, B. B. *ACS Nano* **2014**, *8*, 4295–4303.
- (45) Bryks, W.; Wette, M.; Velez, N.; Hsu, S.-W.; Tao, A. R. *J. Am. Chem. Soc.* **2014**, *136*, 6175–6178.
- (46) Sigman, M. B.; Ghezlbash, A.; Hanrath, T.; Saunders, A. E.; Lee, F.; Korgel, B. A. *J. Am. Chem. Soc.* **2003**, *125*, 16050–16057.
- (47) Espinet, P.; Lequerica, M. C.; Martín-Alvarez, J. M. *Chem.—Eur. J.* **1999**, *5*, 1982–1986.
- (48) Ford, P. C.; Cariati, E.; Bourassa, J. *Chem. Rev.* **1999**, *99*, 3625–3648.
- (49) Lapprand, A.; Bonnot, A.; Knorr, M.; Rousselin, Y.; Kubicki, M. M.; Fortin, D.; Harvey, P. D. *Chem. Commun.* **2013**, *49*, 8848–8850.
- (50) Groeneveld, E.; van Berkum, S.; Meijerink, A.; Donega, C. d. M. *Small* **2011**, *7*, 1247–1256.
- (51) Groeneveld, E.; van Berkum, S.; van Schooneveld, M. M.; Gloter, A.; Meeldijk, J. D.; van den Heuvel, D. J.; Gerritsen, H. C.; Donega, C. d. M. *Nano Lett.* **2012**, *12*, 749–757.
- (52) Wang, L.; He, W.; Yu, Z. *Chem. Soc. Rev.* **2013**, *42*, 599–621.
- (53) Donega, C. d. M. *Chem. Soc. Rev.* **2011**, *40*, 1512–1546.
- (54) Zhuang, Z.; Lu, X.; Peng, Q.; Li, Y. *Chem.—Eur. J.* **2011**, *17*, 10445–10452.
- (55) Tang, A.; Wang, Y.; Ye, H.; Zhou, C.; Yang, C.; Li, X.; Peng, H.; Zhang, F.; Hou, Y.; Teng, F. *Nanotechnology* **2013**, *24*, 355602.
- (56) Wang, Y.; Tang, A.; Li, K.; Yang, C.; Wang, M.; Ye, H.; Hou, Y.; Teng, F. *Langmuir* **2012**, *28*, 16436–16443.
- (57) Busupalli, B.; Kummara, S.; Kumaraswamy, G.; Prasad, B. L. V. *Chem. Mater.* **2014**, *26*, 3436–3442.
- (58) Shi, W.; Zhu, J.; Rui, X.; Cao, X.; Chen, C.; Zhang, H.; Hng, H. H.; Yan, Q. *ACS Appl. Mater. Interfaces* **2012**, *4*, 2999–3006.
- (59) Chen, J.; Wu, L. M.; Chen, L. *Inorg. Chem.* **2007**, *46*, 586–591.
- (60) Xu, C.; Zeng, Y.; Rui, X.; Xiao, N.; Zhu, J.; Zhang, W.; Chen, J.; Liu, W.; Tan, H.; Hng, H. H.; et al. *ACS Nano* **2012**, *6*, 4713–4721.
- (61) Wu, W. Y.; Chakraborty, S.; Chang, C. K. L.; Guchhait, A.; Lin, M.; Chan, Y. *Chem. Mater.* **2014**, *26*, 6120–6126.
- (62) Rivest, J. B.; Jain, P. K. *Chem. Soc. Rev.* **2013**, *42*, 89–96.
- (63) Li, H.; Zanella, M.; Genovese, A.; Povia, M.; Falqui, A.; Giannini, C.; Manna, L. *Nano Lett.* **2011**, *11*, 4964–4970.
- (64) van der Stam, W.; Gantapara, A. P.; Akkerman, Q. A.; Soligno, G.; Meeldijk, J. D.; van Roij, R.; Dijkstra, M.; Donega, C. d. M. *Nano Lett.* **2014**, *14*, 1032–1037.
- (65) Casavola, M.; van Huis, M. A.; Bals, S.; Lambert, K.; Hens, Z.; Vanmaekelbergh, D. *Chem. Mater.* **2012**, *24*, 294–302.
- (66) Groeneveld, E.; Witteman, L.; Lefferts, M.; Ke, X.; Bals, S.; van Tendeloo, G.; Donega, C. d. M. *ACS Nano* **2013**, *7*, 7913–7930.
- (67) Eilers, J.; Groeneveld, E.; Donega, C. d. M.; Meijerink, A. *J. Phys. Chem. Lett.* **2012**, *3*, 1663–1667.
- (68) Sahu, A.; Kang, M. S.; Kompch, A.; Notthoff, C.; Wills, A. W.; Deng, D.; Winterer, M.; Frisbie, C. D.; Norris, D. J. *Nano Lett.* **2012**, *12*, 2587–2594.
- (69) Tang, A.; Yi, L.; Han, W.; Teng, F.; Wang, Y.; Hou, Y.; Gao, M. *Appl. Phys. Lett.* **2010**, *97*, 033112.